MOX-Report No. 90/2021

3D numerical modeling of ground motion in the Valley of Mexico: a case study from the Mw3.2 earthquake of July 17, 2019

Hernandez, V.M.; Paolucci, R.; Mazzieri, I.

MOX, Dipartimento di Matematica
Politecnico di Milano, Via Bonardi 9 - 20133 Milano (Italy)

mox-dmat@polimi.it http://mox.polimi.it

3D numerical modeling of ground motion in the Valley of Mexico: a case study from the Mw3.2 earthquake of July 17, 2019

V. M. Hernandez[1], R. Paolucci[2], and I. Mazzieri[3]

[1]Department of Civil and Environmental Engineering, Politecnico di Milano, Milano, Italy. victormoises.hernandez@mail.polimi.it
[2]Department of Civil and Environmental Engineering, Politecnico di Milano, Milano, Italy. roberto.paolucci@polimi.it
[3]MOX, Dipartimento di Matematica, Politecnico di Milano, Milano, Italy. ilario.mazzieri@polimi.it

December 10, 2021

Keywords : Earthquake ground motion, Site effects, Mexico City basin, High-performance computing, Physics-based numerical simulations, spectral element method.

Abstract

In this study a 3D physics-based numerical approach, based on the spectral element numerical code SPEED (http://speed.mox.polimi.it), is used to simulate seismic wave propagation due to a local earthquake in the Mexico City basin. The availability of detailed geological, geophysical, geotechnical, and seismological data allowed for the creation of a large-scale (60 km $\times$ 60 km) heterogeneous 3D numerical model of the Mexico City area, dimensioned to accurately propagate frequencies up to 1.3 Hz. Results of numerical simulations are validated against the ground motion recordings of the July 17, 2019, Mw3.2 earthquake, which produced peak ground acceleration (PGA) exceeding 0.3g about 1 km away of the epicenter. Results show that for the hill and transition zones of the Valley of Mexico there is a good agreement with records. For the lake zone, the simulated decay trend of the PGV with epicentral distance was reasonably close to the observations, both for the horizontal and vertical components, but synthetics present in general shorter duration with respect to records, probably due to insufficient accuracy of considered values of the quality factor. In spite of these limitations, the simulations proved to be suitable to provide a comprehensive picture of seismic wave propagation in the lake zone of Mexico City, including the onset of long-duration quasi-monochromatic ground motion with strong amplification between 0.5 and 0.6 Hz. The numerical results also suggest that higher-mode surface waves dominate the wavefield in the lake zone of Mexico City, as evident from the measured phase velocities and vertical displacements along vertical arrays. Based on these positive outcomes, we conclude that this numerical model may be used for the simulation of ground motions during larger magnitude earthquakes, for example in view of generation of seismic damage scenarios in Mexico City.

1 Introduction

Mexico has a long history of destructive earthquakes. The September 19, 1985 Michoacán earthquake has been the deadliest in Mexico's history. The main shock, with a magnitude M_S8.1, was caused by the subduction of the Cocos plate beneath the continental plate of North America, in the zone known as the Michoacán gap. The earthquake killed some 10'000 people in Mexico City, left about 50'000 homeless, and produced material losses of about 4 billion dollars, including the collapse of over 200 multistorey buildings [13].

The 1985 Michoacán earthquake was exceptional because, despite peak ground accelerations in the epicentral area were relatively low, still it caused severe damage in Mexico City, about 360 km away. Moreover, shaking duration inside the basin was exceptionally long, with huge differences in intensities of shaking and associated building damage in different parts of the city [40]. While source [46, 47] and path [31] effects were proved to have contributed to the severe long lasting ground motion, various studies have established beyond question that the decisive factor of the 1985 catastrophe in Mexico City was a very large local amplification caused by the shallow geology, e.g., [40, 38, 8], i.e., site effects, caused by the presence at the basin's surface of a very thin, extremely soft clay layer, and the underlying consolidated deposits. In fact, [45] quantified amplification factors as high as 50 at 0,5 Hz in the soft soil zone (lake-bed zone), relative to hard-rock zone (hill zone) motion.

Not only subduction earthquakes, as that of Michoacán, are relevant for the seismic hazard of Mexico City, but also are intermediate-depth intraplate normal-faulting earthquakes. On September 19, 2017, two hours after the city had undergone a macroearthquake drill for the 32nd anniversary of the M_S8.1 Michoacán earthquake, an Mw7.1 intraplate normal-faulting earthquake struck central Mexico, with epicenter 120 km away from Mexico City. This earthquake led to 369 casualties, 228 of them in Mexico City, where 5'765 dwellings were damaged and 52 buildings collapsed.

Local crustal earthquakes are also relevant for the seismic hazard of Mexico City. The Valley of Mexico has a complex geology and tectonics, with numerous mapped active faults within the valley, exceeding 20 km in length [3]. During the period 2010-2020, 12 earthquakes with moment magnitude in the range 3.0-3.6 took place in the Valley of Mexico [54]. Recently, [50] estimated ground motions from an Mw5.0 scenario earthquake in the Valley of Mexico, using as empirical Green's functions the recordings of an earthquake swarm that took place in Mexico City in 2019. Their results reveal that such an event may give rise to significant intensities in the lake-bed zone, and therefore a vigorous research effort is urgent to re-evaluate seismic hazard posed by local crustal earthquakes.

Early attempts to evaluate site effects in Mexico City after the Michoacán earthquake used vertical S-wave propagation models (1D). The use of this model was encouraged because of clay deposits are very thin compared to their lateral extent, coupled with the high impedance contrast between the clay and its basement. Furthermore, the recorded Fourier spectral peaks appear close to the natural periods of the ground. However, while simple 1D models allow to reproduce the spectral amplification between the lake-bed and hard-rock zones in Mexico City, they are unable to elucidate the differences in the duration of strong motion between these areas [38, 8].

Different models have been proposed to explain the long ground motion duration in Mexico City, such as: (1) a 2-D valley [38], (2) a large-scale 2-D valley within which a small-scale lake-bed zone is located [5, 25], (3) lateral variations in thickness of the clay deposits [7],

(4) stochastic variations in the clay deposits shear wave velocity (V_S) [16], and (5) resonance of horizontally propagating P waves in a laterally confined clay layer of the lake-bed zone [41]. 2D numerical models with large-scale and small-scale heterogeneities provide a viable explanation of long coda only when the quality factor (Q_S) for the clay deposits is high (200–300). However, Q_S values in the range 10-50 are more suitable according to laboratory [36] and field [23] measurements. Various authors, e.g.,[48, 6, 42, 43, 20] have suggested that long durations may be attributed to dispersion and multipathing between the source and the Mexico City basin.

From the analysis of records at the ground surface and in boreholes in the lake-bed zone, [44] found that the wavefield in the lake-bed zone is dominated by higher-mode surface waves, that are less affected by the low Q_S values of the surficial clay layer. Furthermore, based on observational evidence from a local Mw3.4 earthquake and from 3D numerical simulations upon application of vertical body forces at the ground surface, [10] studied the factors affecting the long duration ground motions in the Mexico City Valley, and concluded that seismic energy within the deep sedimentary basin is dominated by surface waves overtones that can propagate long distance owing to the rapid decay with depth of the dissipation properties. According to [10]) this mechanism may increase the duration of ground motion by more than 170% and 290% of the incoming wavefield duration at 0.5 and 0.3 Hz, respectively.

With the objective of improving the understanding of the Mexico City Valley seismic response, after constructing a large 3D spectral element model of the Mexico City Valley, this paper is focused on the validation of the numerical model, carried out on the physics-based numerical simulations (PBS) of the July 17, 2019, Mw3.2 Mexico City earthquake (Fig. 1). This earthquake was selected because of the large number of records available in the epicentral area and in the lake-bed zone, and of the relatively large magnitude. Numerical simulations were performed using the code SPEED (Spectral Elements in Elastodynamics with Discontinous Galerkin, http://speed.mox.polimi.it). Compared to other validation tests of PBS carried out by SPEED against near-source records of large magnitude earthquakes in tectonic areas [18, 52, 35, 21], where the largest source of discrepancy comes from both the poorly constrained kinematic extended fault model and from the limited detail of the shallow ground model, in this case the task may be simpler because of the limited fault rupture dimension, that may reasonably be approximated by a point double-couple, and of the detailed site investigations available throughout the Mexico City area. A similar validation benchmark was recently carried out for the induced-seismicity ground motion simulation in the Groningen area, the Netherlands, considering an earthquake of comparable magnitude and with a similarly well detailed geological model [34]. However, while the dimensions of the Groningen model were reasonably small (20 km x 20 km in plan) and the challenge was an extension to high frequencies (f_{max}=8 Hz), the most challenging aspect of the validation within the Valley of Mexico is probably the ability of PBS to produce a reasonably good approximation of records in a frequency range as extended as possible considering the extremely low V_S in the lake-bed zone and the large overall dimension of the model (60 km x 60 km in plan).

As previously mentioned, a large-scale 3D numerical model for Mexico City was presented by [10]). While the dimensions and maximum resolvable frequency of our model are similar to those of [10], we introduced a more detailed V_S vertical distribution and a variable thickness of the clay deposits based on the contour map presented by [24].

The paper is organized as follows. After a description of the set-up of the 3D numerical model (3) based on the vast geological, geotechnical and geophysical data available for Mexico

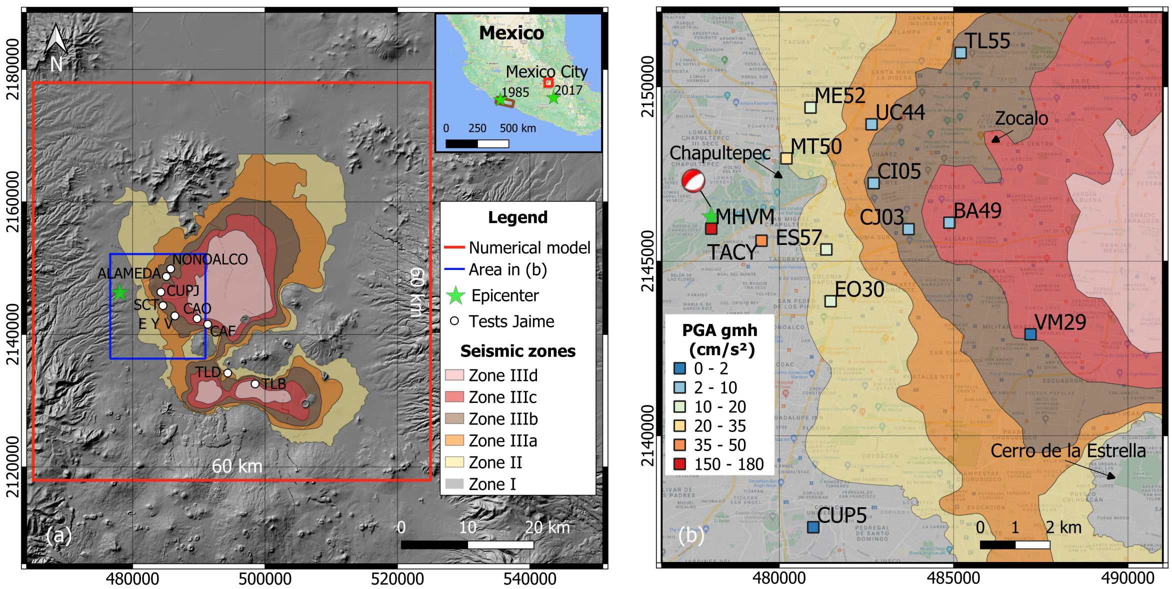

Figure 1: (a) Portion of the Valley of Mexico covered by the 3D numerical model (red box, 60 km x 60 km in plan). The star indicates the epicenter of the Mw3.2 Mexico City earthquake (17.07.2019). Seismic zones according to the Mexico City building code are also presented, Zone I=Hills, Zone II=Transition, Zone III=Lake-bed. White dots represent the locations of the V_S profiles in Fig. 3. In the upper part, a portion of Mexico is presented showing the area covered by the 3D numerical model and the epicenters of the 1985 M_S8.1 Michoacán and 2017 Mw7.1 Puebla earthquakes. (b) Zoom to a portion of the model (blue box in a) showing the considered stations that recorded the Mw3.2 earthquake (with the related fault mechanism), with the corresponding geometric mean of horizontal components (GMH) of peak ground acceleration.

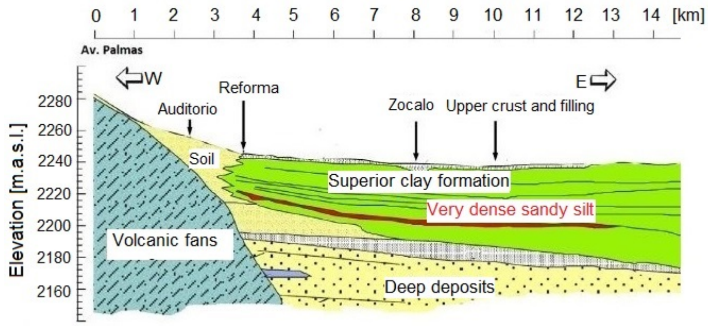

Figure 2: Typical stratigraphic sequence of Mexico City. Adapted from [39].

City (2), the case study of the July 17 Mw3.2 earthquake is presented (4). Then, after a verification test with an independent solution (5.1), a calibration of the slip function and of V_S for the shallowest part of the hill zone is carried out (5.2). Finally, numerical results are compared with records (5.3) and the effect of Q_S for the clay deposits is evaluated (5.4). The sensitivity analysis was limited to Q_S because it is the parameter with the largest uncertainty and because of the large computational demand for the simulations. Some characteristics of the wave propagation in the Valley of Mexico are also discussed (6).

2 Integration of the available geological, geotechnical and geophysical data

Mexico City is located on a volcanic plateau at about 2240 m above the sea level, surrounded by volcanic sierras, alluvial fans and plains. By the end of the Pliocene important fractures arose predominantly EW, and gave rise to basaltic effusions of the Chichinautzin mountain range, which transformed the valley into a closed basin during the Quaternary [39]. Afterwards, the bottom of the basin was silted up with a stratification of different type of materials, like proluvials, lacustrine materials, volcanic sand and ash that, upon weathering, generated highly compressible clays [4]. Therefore, Mexico basin presents two main geological units overlying the pre-Chichinautzin basement, i.e., a thick consolidated unit, forming the so-called "deep deposits", overlaid by a thin clay formation with very poor mechanical characteristics (Fig. 2). In 1519, when the Spanish arrived to Tenochtitlan (nowadays Mexico City), there were five lakes within the basin. After a series of floodings, the lakes were drained, and the city extended on the former lake-bed.

Mexico City clays present notoriously high Atterberg limits and natural water contents, that in some parts of the city can reach values as high as 600%. These materials have been pointed out as extremely plastic clays which, correspondingly, display very low shear strengths and rather large compressibilities [32].

On the basis of geotechnical characteristics, Mexico City is divided into three main zones, according to the Mexico City Building Code [17]:

Zone I. Hills, formed by rocks or hard soils that were generally deposited outside the lake area, but where sandy deposits in relatively loose state or soft clays can also be found.

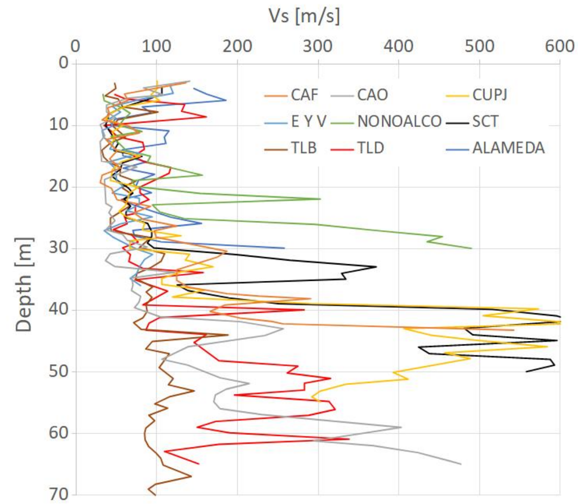

Figure 3: V_S profiles obtained from down-hole and P-S suspension logging tests carried out in the lake-bed zone [22]. The location of the test is presented in Fig. 1a.

Zone II. Transition, where deep firm deposits are found at a depth of 20 m or less and consisting predominantly of sand and silt layers interbedded with lacustrine clay layers.

Zone III. Lake, composed of potent deposits of highly compressible clay strata, separated by sand layers with varying content of silt or clay.

The seismic zonification of Mexico City (Fig. 1), is similar to the geotechnical zonification, the main difference being that the zone III is further subdivided into zones IIIa, IIIb, IIIc and IIId, to account for the increasing depth of the clay deposits when moving from the hill zone to the center of the old lakes. After the Michoacán earthquake, a thorough study of the Mexico City clays' dynamic properties was carried out [22, 37, 11, 36]. One of its main characteristics is that due to its high plasticity index, they exhibit no significant reduction in shear modulus even for shear strains as high as 0.1%. Similarly, there is no significant increase in the damping ratio until angular distortions of the order of 0.3% [37, 28].

Mexico City clays are characterized by very low V_S, usually lower than 100 m/s. Fig. 3 shows results from down-hole and P-S suspension logging test carried out in the lake-bed zone [22], from which V_S as low as 40 m/s were measured, and clay deposis with maximum thickness reaching about 70 m were found (e.g., site TLB in Fig. 3). Furthermore, the impedance contrast with the deep deposits is evident: for instance, for sites SCT ans CUPJ there is a sudden increase of V_S to 600 m/s at around 40 m depth. Differently, due to its large Poisson's ratio (~0.49), Mexico City clays present a large V_P [**?**, e.g.,]]Jaime1987,Perez-Cruz1988,Jongmans1996, in the range of 700-1600 m/s.

On the other hand, the available information on the deep deposits is scarce. From some deep boreholes carried out by PEMEX in 1987 (Pérez-Cruz, 1988), it was found that the deep deposits reach depths as large as 500 m. [27] presented the results of seismic refraction tests carried out in the former Texcoco lake, in which the contact of the deep deposits with the pre-Chichinautzin basement was found at depths between 250-500 m. They also measured a V_P of 1550-1700 m/s for these materials. [22] measured a V_S between 350-600 m/s in the first meters of the deep deposits.

3 Set-up of the 3D numerical model for the Valley of Mexico

3.1 The Spectral Element Code SPEED

3D physics-based numerical simulations of seismic wave propagation in the Valley of Mexico were carried out using the open-source computer code SPEED, suitable for the simulation of seismic wave propagation including the coupled effects of the seismic source and the propagation path through heterogeneous Earth's media [29]. Based on the Discontinuous Galerkin Spectral Element (DGSE) formulation [2], the code can handle non-conforming grids (h-adaptivity) as well as variable approximation orders (N-adaptivity), making them suited for simulations with adaptive choice of discretization parameters.

In its present version, SPEED allows the user to treat different seismic excitations, including kinematic (either double couple point source or extended fault) and dynamic rupture models, as well as plane wave propagation. Moreover, different anelastic attenuation models are available to model linear viscoelastic material behavior, specifically: (a) frequency-proportional quality factor Q [26]; (b) hysteretic Q (independent on frequency), as in the Generalized Maxwell body [12], and (c) the classical Rayleigh damping. Finally, a nonlinear elastic constitutive rheology is also implemented [56]. Besides being verified over different benchmarks [29] and validated against recordings of past earthquakes, such as the April 6, 2009, L'Aquila, Central Italy [14], and the May 29, 2012, Po Plain, Northern Italy [35], SPEED has proved to be an effective tool, complementary to empirical GMMs, for seismic hazard and risk assessments in large urban areas [51, 55]. To pursue this objective, a dataset of broadband near-source accelerograms simulated by SPEED has recently been compiled [**?**, BB-SPEEDset,]]Paolucci2021b, aiming at complement the still relatively sparse availability of near-source records from earthquakes at a global scale.

3.2 The subsoil model

Two 3D surfaces were created representing the base of the clay deposits and deep deposits, from the digitalization of the contours proposed by [24] and [10], respectively.

For the crustal structure surrounding the basin, a 1D model determined from the inversion of receiver functions at the CU site [9] was adopted (Crust materials in Table 1). Quality factors Q_S for the crustal materials are taken equal to $V_S/10$, which is in accordance to typical values considered in literature [35, 10], while Q_p is considered as $2{\cdot}Q_S$. Considering that, shallow deposits of tuffs intercalated with sands, gravels and recent lava flows are found on top of the Oligocene volcanics rocks [49], after the calibration presented in Section 5.2, we introduced a shallow layer of V_S=750 m/s for the first 200 m of the hill zone. The dynamic properties of the horizontal crustal layers are shown in Table 1.

For the Mexico City clays, the use of a linear visco-elastic model is considered to be adequate since they exhibit no significant reduction in shear modulus even for shear strains as high as 0.1% [37]. Considering that Q_S for the clay is in the range of 10-50, according to laboratory [36] and field measurements [23], three damping models are considered, as shown in Table 2, the effect of which will be discussed in a subsequent section.

Table 1: Geological interfaces and soil profile properties of the 3D numerical model.

Material	Geological interface	Thickness H [m]	V_S [m/s]	V_P [m/s]	ρ [kg/m^3]	Q_S [-]	Q_p [-]
Basin 1	Base of the clay deposits	0-100	70-100	910-1300	1400-1600	Table 2	$2{\cdot}Q_S$
Basin 2	Pre-Chichinautzin	0-500	Fig. 4	Fig. 4	1900	$V_S/7$	$2{\cdot}Q_S$
Crust 1	TMVB basement	200 1800	750 1550	1700 2782	2000 2200	100 155	200 310
Crust 2	Marine formations (Morelos and Mexcala)	2300	3150	5624	2530	315	630
Crust 3	Pre-Mesozoic metamorphic basement - Halfspace	6000	3500	6283	2700	350	700

Table 2: Overview of the physics-based numerical simulations performed in this study to simulate the 2019 Mexico City earthquake.

Label simulation	Q_S for clay deposits [-]	Duration [s]	Cores	Wall time [h]
3D-Qf	Freq. proportional $22.3<Q_0<33.3$ (0.9 Hz)	32	512	90
3D-Qh	Hysteretic, $35<Q<50$	25	512	74
3D-Qh2*	Hysteretic, $40<Q<55$	35	1024	26

*Mesh for simulation 3D-Qh2 differs slightly in clay thicknesses to that used for the first two simulations.

The variation of shear wave velocity with depth for the clay deposits was defined based on the results presented in Figure 3. In order to account for the increase in V_S due to regional subsidence since the date in which the tests were carried out, V_S values were increased by 16%, in accordance with the increase in $\sqrt{G_{max}}$ estimated by [33]. For every location (x_i,y_i), it was considered a linear variation of V_S from 70 m/s at the ground surface to 100 m/s at the contact with the deep deposits. Here, P-wave velocity for the clay is adopted as V_P=13$\cdot V_S$, which corresponds to a value of Poisson's ratio of $\sim$0.49, that is common for the dynamic response of Mexico City clays [22].

As for the deep deposits, $V_S = 500 + 9.6 \cdot z^{0.6}$ and $V_P = 1500 + 19.2 \cdot z^{0.6}$ (Fig. 4). The dynamic properties for the clay deposits are presented in Table 1 as material Basin 1, while the properties for the deep deposits are shown as material Basin 2.

3.3 Mesh features and computational resources

Once all the dynamic parameters have been defined, the mesh is designed to limit the numerical dispersion by the condition $\Delta l \leq \lambda_{min}/G_\lambda \cdot N$, that defines the maximum spectral element size (Δl) as a function of V_S, N (degree of the spectral interpolant polynomial) and f_{max} (maximum frequency to be propagated), the latter one limited to 1.3 Hz in order to avoid computational overburden. Based on [15], G_λ=4 is considered.

The mesh was created using the software CUBIT (http://cubit.sandia.gov). It extends over a volume of about 60 x 60 x 10 km^3 and it is discretized using an unstructured hexahedral conforming mesh. The basin, i.e., clay and deep deposits, is modeled using the not-honoring

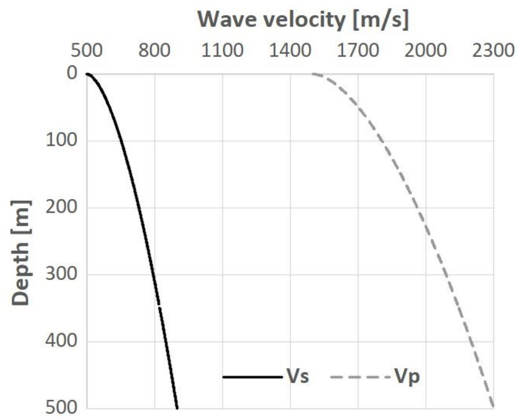

Figure 4: Variation with depth of V_S and V_P for the deep deposits.

technique, according to which SPEED evaluates whether a node in the spectral element is located within the basin: if so, it assigns the properties of the basin material, otherwise those of the adjacent crustal layer. The basin lies within the mesh block 1, which has an area of $\sim$1650 km^2 and 500 m height, and characteristic element size Δx of 100 m. The crustal materials (blocks 2, 3 and 4) are meshed with Δl going from 300 m to 2700 m at the base of the model. The configuration of the mesh, which consists of 2'446'082 spectral elements and results in approximately 308.7x10^6 total degrees of freedom, is summarized in Fig. 5.

Cross-section A-A' (red dashed line in Fig. 5) is presented in Fig. 6 with V_S values assigned to the numerical model.

3D physics-based numerical simulations were performed on the Marconi100 high performance computing cluster located at CINECA, Italy (www.hpc.cineca.it), with the number of cores and wall times presented in Table 2. For all simulations a time step Δt=2$\cdot$10^{-4} s was chosen, which is around 21% of the CFL condition for numerical stability.

We want to point out that the numerical model solution requires the use of a scalable code that allows the efficient use of high performance computing architectures. If compared to more classical approaches, such as GMPEs, numerical techniques of this kind are much more demanding from a computational point of view. Nevertheless, the large amount of data obtained from physics based models can help to better understand the observed phenomenon, as we will explain in the next sections.

4 Case study: The July 17, 2019 Mw3.2 Mexico City earthquake

The case study is the largest event of the earthquake swarm activity, which occurred between July 12 and July 18, 2019, in the borough Miguel Hidalgo, at the western part of Mexico City. The Mexican Seismological Service [53] reported 20 shocks during that week with magnitude in the range 2.0-3.2. The largest event of the sequence, an Mw3.2 earthquake, took place at 03:59 h (22:59 h local time) on July 17, with epicenter at 19.4090° N, 99.2090° W and depth of 800 m (Fig. 1), as reported by [50]. The sequence was recorded by several stations operated by different Institutions (SSN, IINGEN and CIRES). Despite the magnitude of this earthquake

Material	Block	V_S [m/s]	N	Δx [m]	No. elements	No. LGL nodes
Basin 1 & 2	1	70-900	5	100	1'229'094	153.6x10^6
Crust 1	2	750-1550	5	300	1'203'452	153.4x10^6
Crust 2	3	3150	5	900	12'408	1.55x10^6
Crust 3	4	3500	5	2700	1'128	0.15x10^6

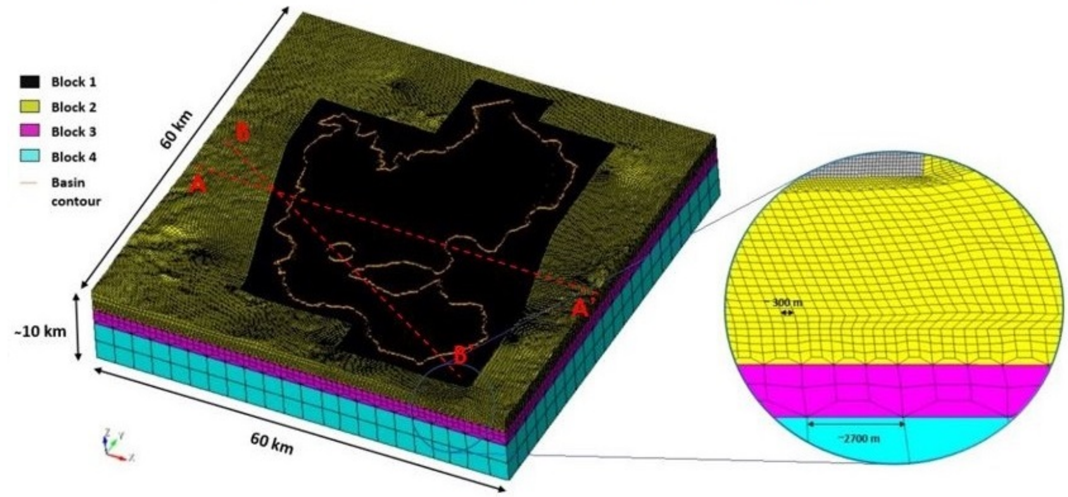

Figure 5: 3D mesh for the Mexico City area consisting of 2'446'082 spectral elements with N=5.

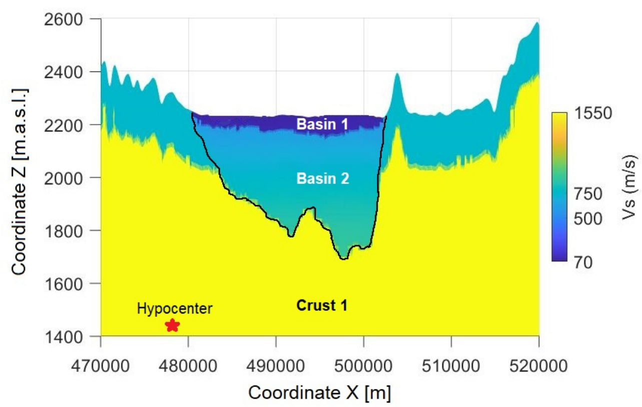

Figure 6: Cross-section A-A' (whose location is shown in Fig. 5) showing V_S values assigned to the 3D numerical model.

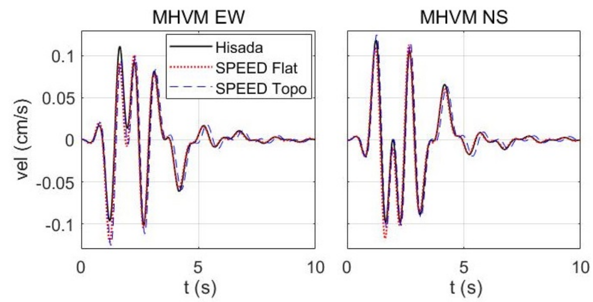

Figure 7: Comparison between Hisada (black solid line) and SPEED (dashed lines) results using a horizontally layered model, considering a point source. The agreement between SPEED and Hisada is evident. Numerical results have been low-pass filtered at 2 Hz.

was low, it caused panic in the city and produced PGA exceeding 0.3 g (E-W component) at the closest station (MHVM, see Fig. 1 for location), which is the largest ever recorded at a hill-zone site in the Valley of Mexico. [50] have suggested that the high PGA resulted from high-frequency amplification at MHVM (about factor of 6 around 1 Hz), possibly due to topographic site effects.

The focal mechanism for this event was obtained by [50] from the moment tensor inversion of band-pass filtered (0.08-0.2 Hz) displacements, yielding Mw=3.2, striking $\varphi = 228°$, dip $\delta = 80°$, and rake $\lambda = -97°$.

5 Physics-based numerical simulations of the earthquake case study

5.1 Verification test against an independent solution

As a preliminary step of the modelling process, a verification test of SPEED results was performed with an independent numerical code (Hisada), based on the analytical integration of Green's functions [19]. For this purpose, a horizontally layered model based on the crustal materials in Table 1 was used (i.e., without considering the basin). A point seismic source was introduced, considering that this approximation is generally valid for distances larger than the size of the fault as well as the wavelength of interest. In Fig. 7, the results for station MHVM from the Hisada simulation (solid line) are compared to those from two SPEED simulations, one having a flat ground surface (SPEED Flat, dotted line) and the other one including the ground topography (SPEED Topo, dashed line). Simulations were limited to 2 Hz. The agreement between the two SPEED solutions and Hisada is evident, proving, on one side, the accuracy of the SPEED code in the selected frequency range and, on the other side, that in such range the topography effect does not play a significant role.

5.2 Calibration with hill zone records

A calibration process was carried out in order to define two important parameters to be used in the 3D simulation of the July 17, 2019 earthquake ground motion with SPEED, namely: (1) the slip rate function of the point source; and (2) the V_S for the shallowest part of the crustal

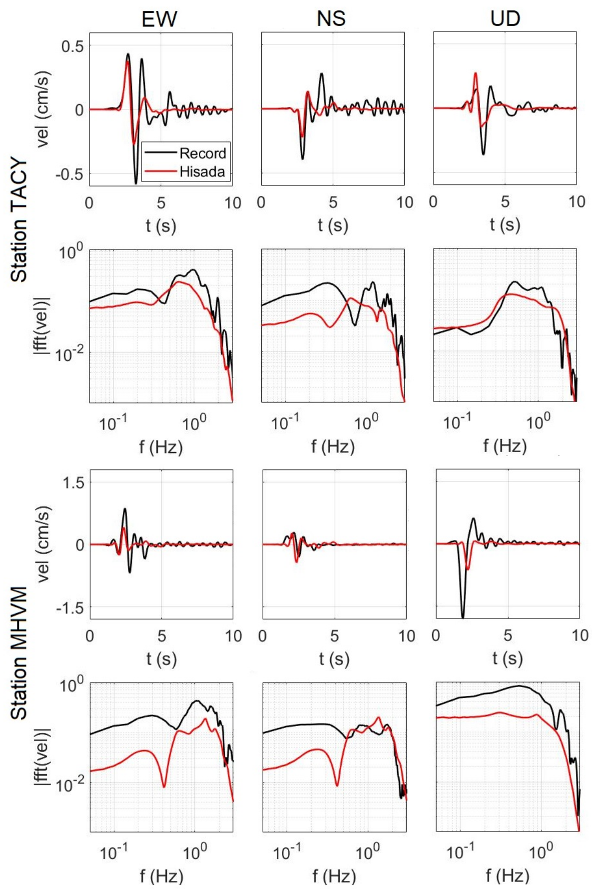

Figure 8: Comparison with records (black lines) at stations TACY and MHVM (located at the hill zone), of the results from Hisada (red lines) using the focal mechanism by [50], an exponential slip function with τ=0.2 s, and V_S=750 m/s in the shallowest 200 m. A good agreement with records was obtained using these parameters. Numerical results and records have been low-pass filtered at 2 Hz.

model. This was accomplished by computing synthetics using the code Hisada, changing the values for both parameters until the best agreement of synthetics with records was obtained (Fig. 8). From this process, it was decided to use a slip rate function represented by equation $s(t) = t \cdot exp(-t/\tau)/\tau^2$, with τ=0.2 s. Regarding the V_S profile for the hill zone, the best agreement with records was obtained by assigning V_S=750 m/s to the first 200 m.

5.3 Validation against records

In this section the results from simulation 3D-Qh2 are presented, which uses a hysteretic Q-factor with larger values for the clay deposits than simulations 3D-Qh and 3D-Qf (see Table 2), that allowed to obtain the best agreement to the recorded values. Besides, in the 3D-Qh2 simulation, a special care was taken to modify locally the clay thickness especially in the transition zone, because the automatic 3D meshing technique provided in some areas values distant from the actual ones. Fig. 9 shows a comparison of recorded and synthetic ground

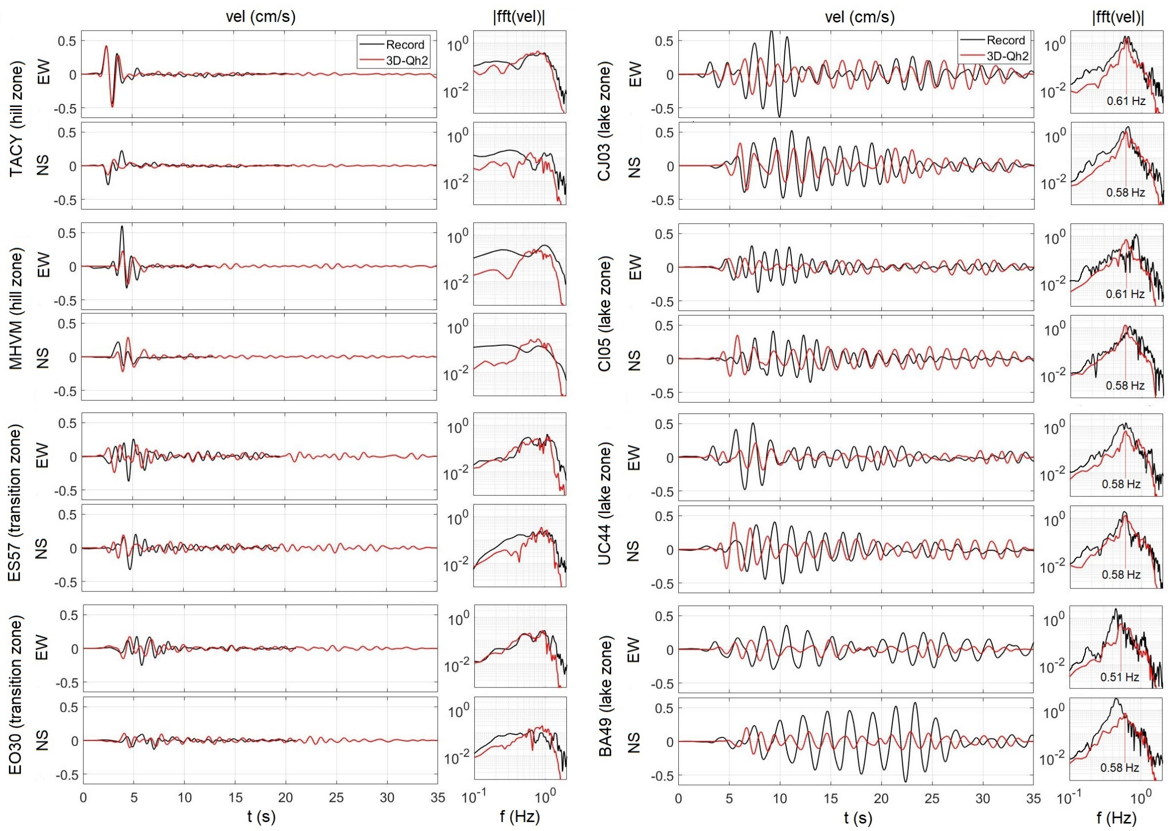

Figure 9: Comparison between recorded (black lines) and computed (from 3D-Qh2 simulation, red lines) velocity time-histories and their corresponding FAS, at some selected stations. Numerical results and records have been low-pass filtered at 1.3 Hz.

motions at some selected stations. Both numerical results and records have been low-pass filtered at 1.3 Hz, for consistency with the spatial resolution of the numerical mesh. As shown in Fig. 9, for the hill and transition zones a good agreement between synthetics and records is generally found, both in time and frequency domains.

As for the lake zone, the simulated ground motions reproduce reasonably well the most important features of the ground motion in Mexico City, namely: (1) the long-duration quasi-monochromatic ground motion, and (2) the strong amplification between 0.5 and 0.6 Hz, as evident in the Fourier spectra, with in general lower amplitudes.

The overall performance of the numerical results was quantitatively estimated through the Goodness-of-Fit (GoF) criteria [1], considering only the peak parameters of ground motion of interest for earthquake risk applications, namely: PGA, PGV, Peak Ground Displacement (PGD) and Spectral accelerations (Sa) at periods T=0.5, 1, 1.5, and 2 s. The final GoF scores, shown in Figure 10 in terms of the geometric mean of the horizontal components (GMH), were computed as an equal-weighting average of the selected metrics [35].

Although GoF scores are overall rather satisfactory, with only few exceptions (such as stations GR27, VM29, TL55, all of them at large epicentral distances), in the interpretation of these results it should be recalled that the 3D PBS are expected to provide an overall realistic picture of the space and time evolution of the earthquake ground motion in a given

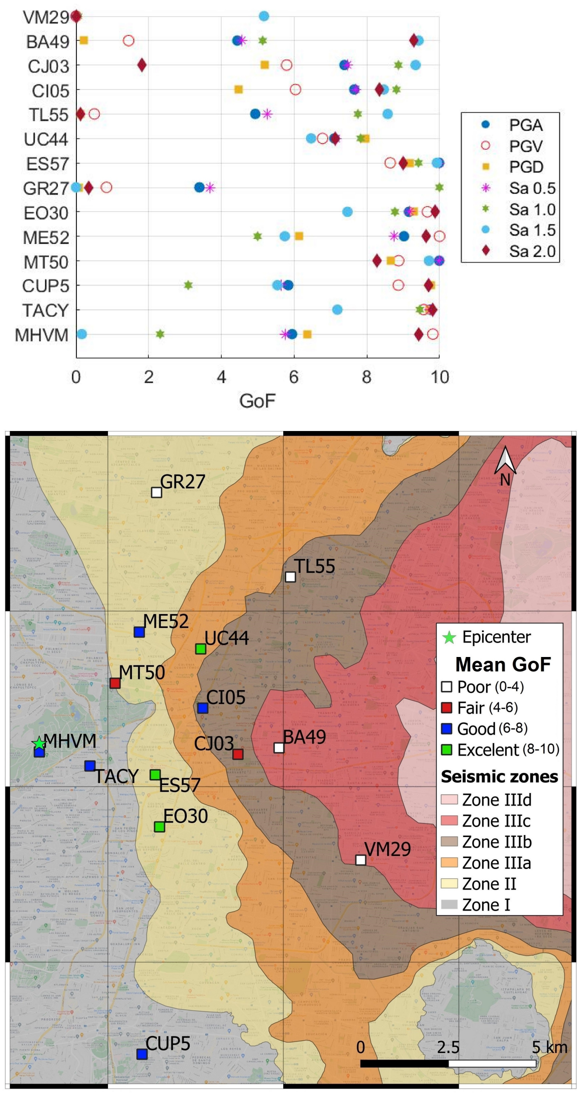

Figure 10: Above: GoF scores computed on the geometric mean of the horizontal components of PGA, PGV, PGD, and Spectral acceleration at T = 0.5, 1.0, 1.5, and 2.0 s. Below: map of the mean GoF scores.

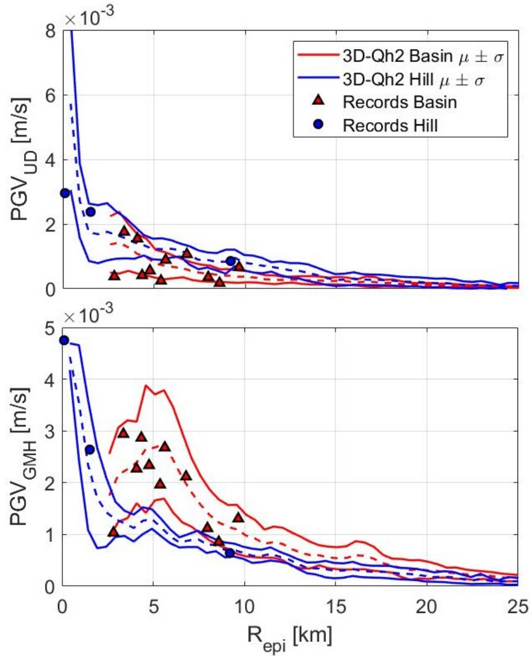

Figure 11: Comparison of variability bands of PGV of numerical simulation 3D-Qh2 (lines) with records for the basin (red) and hill zone (blue). Top: U-D and bottom: GHM components.

area, rather than a very accurate prediction at a specific receiver. As a matter of fact, the 3D model cannot be in general detailed enough to portray accurately the source-to-site propagation path as well as the details of the local stratigraphy.

In spite of such limitations in terms of the agreement with records of specific stations, Figure 11 shows that the trend with epicentral distance (R_{epi}) of recorded ground motion, expressed in terms of PGV (GMH: geometric mean horizontal), is very well captured by the 3D PBS results. The coloured symbols represent the records, whereas the lines represent the mean (μ) and standard deviation (σ) bands computed from the complete set of SPEED receivers at ground surface from simulation 3D-Qh2. The following remarks can be made:

- the peak values and the decay trend with R_{epi} is reproduced rather accurately by the numerical simulation, both for the basin and for the hill zone;

- as expected, for the GMH component, SPEED results and records for the hill zone are always smaller than those for the basin for the same R_{epi};

- a consistent increasing trend of PGV$_{GMH}$ with R_{epi} from 2.5 to 5.5 km is found for the basin, both on records and in SPEED results, as expected because of the change from the transition zone to the lake-bed as distance from the basin contour increases;

- for the hill zone the vertical (U-D) component is generally larger than the GMH component during the first 10 km, while the opposite happens for the basin.

This points to one of the main advantages of 3D PBS, that is the possibility to generate realistic earthquake ground motions in large areas, both in time and space domain, that

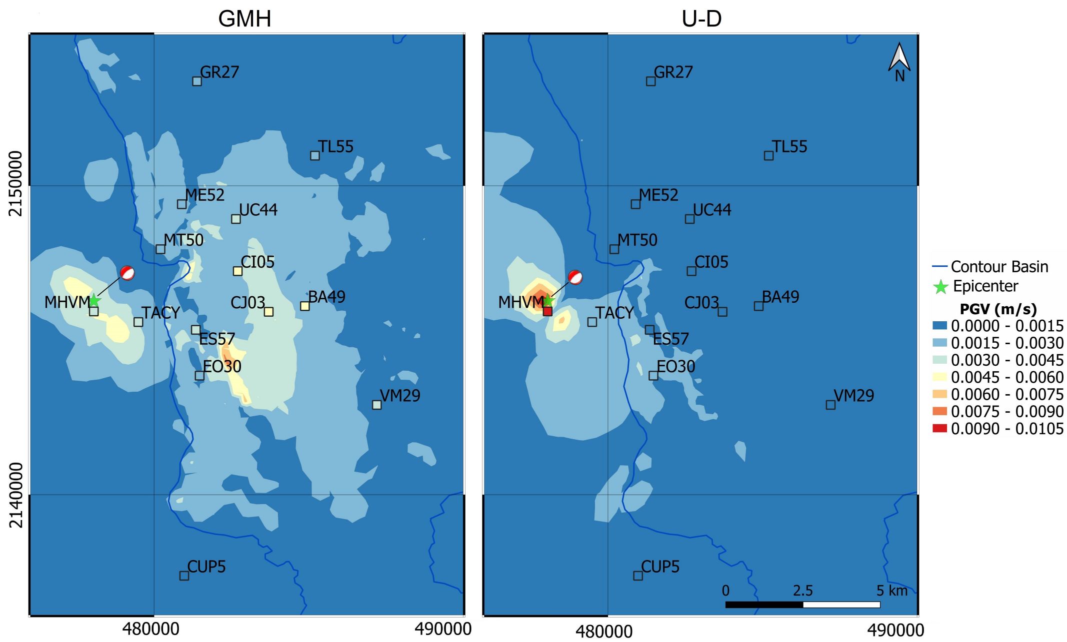

Figure 12: Ground motion maps in terms of PGV for the U-D (right) and geometric mean of horizontal components (left). Recorded peak values are shown by the coloured squares (with the same colour map of simulations). Maps were produced using a grid of around 10,000 simulated motions.

cannot be obtained even by relatively dense recording station networks as the one installed in Mexico City. As an example, Figure 12 shows maps of peak ground velocity (PGV) for the GMH and U-D components of motion, with the corresponding peak values recorded at the same stations (in coloured squares). Besides pointing out a reasonably good agreement between records and the mapped simulated values, it should be noted that, in the near field of the seismic source, a two-lobed radiation pattern is evident, that causes large amplitudes in the direction perpendicular to the fault's strike.

5.4 Effect of Q-factor

As previously mentioned and summarized in Table 2, three linear visco-elastic models were considered in our simulations to investigate their impact, especially in the lake zone, on the ground motion amplitude and duration. Unfortunately, owing to computational resource limits, it was not possible to carry out a comprehensive parametric analysis.

While model 3D-Qf consists of a frequency proportional Q-factor defined as $Q = Q_0 \cdot f/f_0$, where f_0=0.9 Hz and Q_0 is in the range denoted in Table 2, both 3D-Qh and 3D-Qh2 consist of an hysteretic model with Q values independent of frequency and slightly increased from 3D-Qh to 3D-Qh2. It should also be noted that, while the 3D-Qf and 3D-Qh numerical meshes are identical, some slight adjustments were made in the definition of depth of the clay deposits in the transition zone of the 3D-Qh2 numerical model.

Fig. 13 shows a comparison with records of the simulation results at selected receivers: ES57 in the transition zone and UC44, CJ03 in the lake zone (see Fig. 1 for the stations

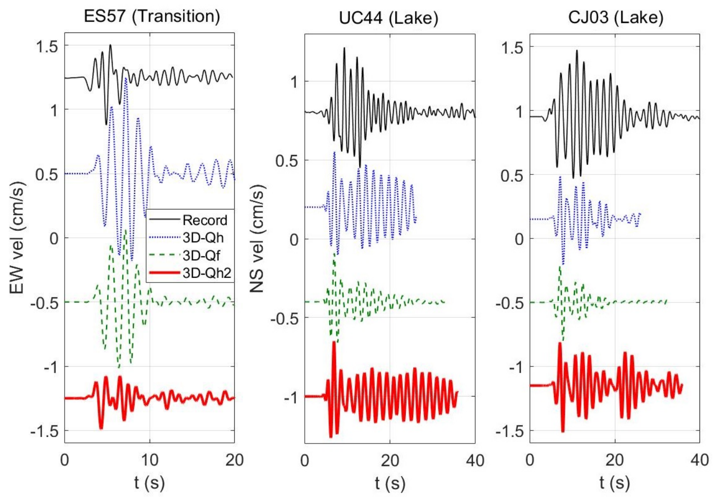

Figure 13: Comparison between results from simulations 3D-Qf, 3D-Qh, and 3D-Qh2, for stations ES57, UC44 and CJ03.

location). The comparison at ES57 clearly shows the importance of capturing accurately the depth of the clay deposits in the transition zone (that was obtained with 3D-Qh2 model), a goal that is not easy to be achieved by a 3D numerical model where relatively sharp lateral geological variations occur.

As for the selected stations in the lake zone, it is concluded that the 3D-Qf model is not adequate, leading to a significant underestimation of ground motion duration, because the frequency-proportional damping implies too low Q-values in the low frequency range, below about f_0. Instead, relatively minor differences are obtained in the lake zone stations for the 3D-Qh and 3D-Qh2 models, mostly due to the slight increase of Q in 3D-Qh2, showing that the adjustment of soil deposits depth in the transition zone has only minor effects in the results obtained in the lake zone.

6 Features of the seismic wave propagation

In this section, some features of the seismic wave propagation within the Mexico City basin will be illustrated with some results from simulation 3D-Qh2. Velocity snapshots for the E-W component at the free surface are shown in Fig. 14, from which different phenomena are observed, such as diffraction (also related to topography irregularities, such as Cerro de la Estrella), amplification within the basin, topographic scattering (especially in the hill zone), and generation of surface waves at the basin edges. Trains of waves traveling at different speeds are also evident.

Fig. 15 shows normalized seismic profiles of the E-W displacement (radial component) at 0.5 Hz, along cross-section A-A' . After the direct S-wave arrivals, prominent waves propagating with a phase velocity of $\sim$1400 m/s are clearly distinguished. Considering the Rayleigh waves dispersion curves for representative 1D profiles within the basin, this train of waves most probably corresponds to the first overtone. Clearly as distance to the basin border and time increase, the ground shaking becomes more erratic, as there is a complex interaction

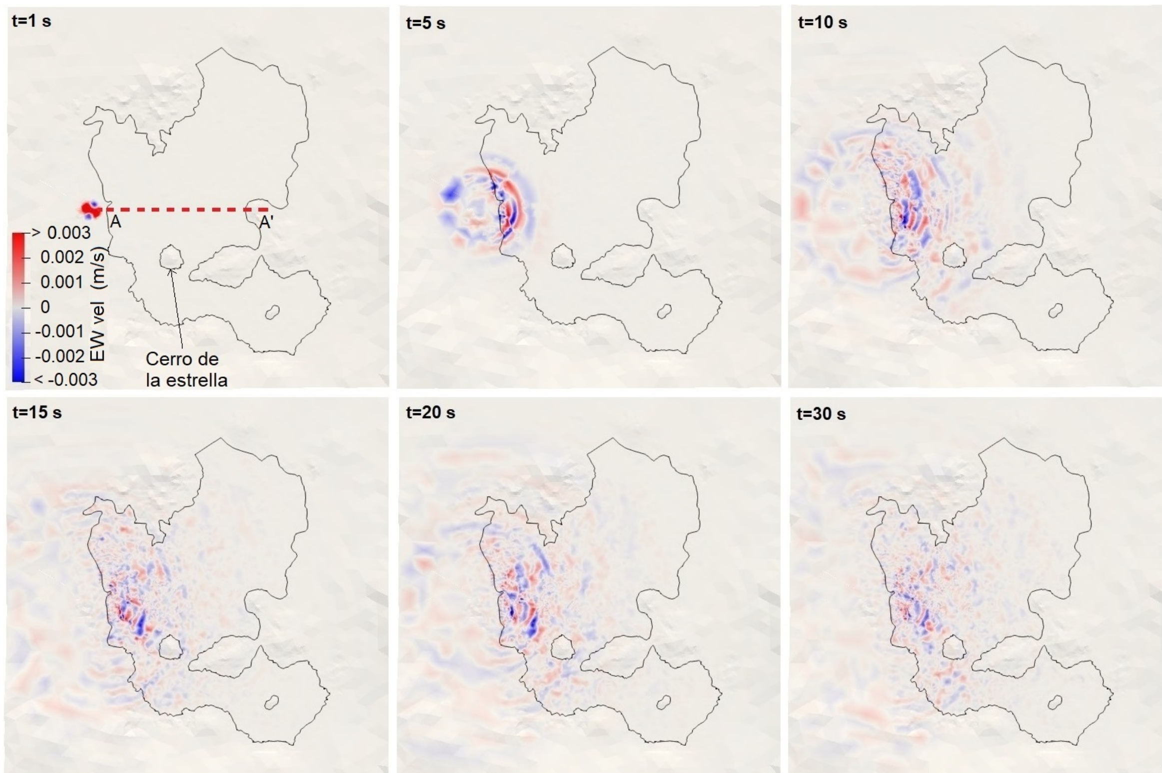

Figure 14: Snapshots of E-W velocity field. Amplification within the basin is clearly observed.

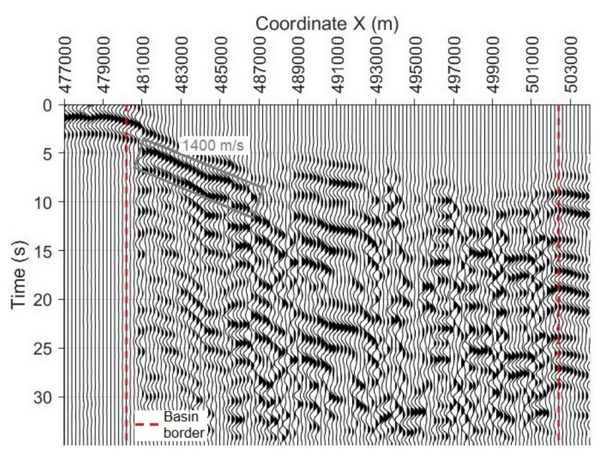

Figure 15: Normalized seismic profiles of the E-W displacement at 0.5 Hz along cross-section A-A'.

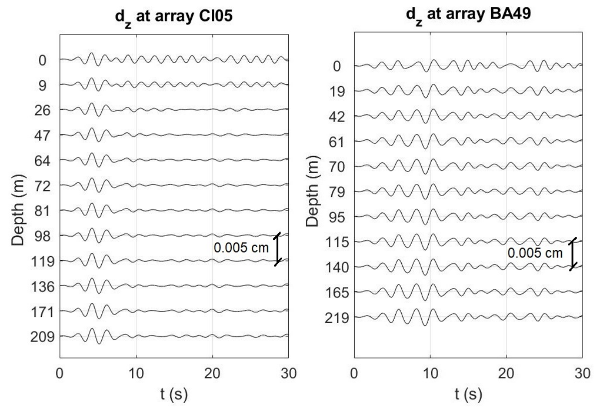

Figure 16: Variability with depth of vertical displacements, d_z, for simulation 3D-Qh2 (at 0.5 Hz), for the arrays CI05 and BA49. The amplitude of displacements remains nearly constant with depth, suggesting that higher mode surface waves dominate the ground motion within the basin.

between different wave types.

Vertical displacements, d_z, at 0.5 Hz were extracted from two vertical arrays, CI05 and BA49. As shown in Fig. 16, the d_z for the first most prominent wave train (before 10 seconds) remains nearly constant with depth for the two arrays, which suggest that this train possibly corresponds to a Rayleigh wave higher-mode.

7 Conclusions

The open-source code SPEED was used to produce 3D physics-based numerical simulations of seismic wave propagation in the Mexico City area. After selection of a 60 km $\times$ 60 km area, down to 10 km depth, including the epicenter of the Mw3.2 Mexico City earthquake on July 17, 2019, a 3D model of seismic wave velocity and quality factor was constructed, based on the vast existing geological and geophysical investigations. The numerical model was designed to propagate frequencies up to about 1.3 Hz, a level of accuracy that implied 308.7x10^6 degrees-of-freedom of the numerical mesh. Even though the maximum frequency is relatively low, it allows to model the main features of the ground motion in the Mexico City basin, governed by the clay deposits, the underlying deep consolidated deposits, and the most important topographic features (such as Cerro de la Estrella).

After verification with an independent solution and calibration of a kinematic source model, the SPEED results were validated against records of the selected local earthquake. For the hill and transition zones, a good agreement was found between numerical results and records, with GoF scores from good to excellent in most stations. As to the results for the lake zone, synthetics present in general lower amplitudes, especially for the stations far away from the basin border. This highlights the role of a more accurate estimate of the Q_S factor within both the shallow and deep basin, that was likely underestimated within our calculations. Due to the large computational demand of the numerical simulations, it was not possible to further extend the sensitivity analysis to evaluate the effect of Q_S, although it is the parameter with the largest uncertainty. As regards the frequency-dependence, the hysteretic (frequency-independent) Q-factor was found to be better suited to predict the extremely long duration of ground motion in the lake zone.

In spite of these limitations, it was shown that physics-based simulations allow to model some important characteristics of the ground motion in Mexico City, namely: (1) the long-duration quasi-monochromatic ground motion, the (2) the strong amplification between 0.5 and 0.6 Hz, and (3) the PGV decay trend with R_{epi}, both for the basin and the hill zone.

Finally, we have shown some evidence suggesting that higher-mode surface waves generated at the basin edges dominate the ground-motion within the basin, as highlighted in the past (e.g., Shapiro et al., 2001; Cruz-Atienza et al., 2016). The main difference between fundamental and higher mode is that energy of the fundamental model is concentrated in the superficial clay, while the higher modes propagate mainly in the deep deposits, where the attenuation is lower, hence, they can propagate longer distances inside the basin. Therefore, the effect of the dynamic properties of the deep basin should be relevant. Furthermore, since dynamic properties for the deep deposits are poorly known, and the parameters used in the simulations were assigned based on few experimental results available on the literature, a better characterization of the deep deposits is needed.

After this validation phase, we have shown that, using 3D physics-based numerical modeling, it is possible to generate synthetic ground-motions in the Mexico City area, within a sufficiently large range of frequencies, suitable to predict the main features of wave propagation that characterize its exceptional seismic response. Therefore, the numerical approach presented in this study may be used to generate physics-based ground shaking scenarios from future local earthquakes affecting Mexico City and resulting from hypothetical and mapped fault breaks within the Mexico Valley.

Larger computational domains might be considered to perform numerical simulations of subduction earthquakes, such as that of Michoacán that devastated Mexico City on Sep 19, 1985. Although simulating such earthquake ground motion would be one of the most appealing targets for these 3D PBS, the computational load is still presently beyond the resource limits that we could have access during this work. However, as discussed by [30] with reference to earthquake motion physics-based simulations, the performance of computing platforms is growing exponentially and this limit is expected to be overcome in relatively short time. This will lead to several potential applications relevant to the seismic risk assessment in the Mexico City area, and, more generally, to a variety of earthquake engineering problems, such as:

- providing relevant ground-motion scenarios, with different magnitude and seismic source, to be used to define potential damage scenarios for civil protection applications, as well as input for nonlinear time history analyses to determine area-specific fragility curves for buildings in Mexico City;

- calibrating simulation-based area-specific spatial correlation models, fundamental for seismic risk assessment of spatially-distributed portfolios; and

- providing simulated waveforms preserving the spatial coherency of ground motion in a broad frequency range, useful for the seismic analysis of spatially extended structures and infrastructures.

Acknowledgments

The authors extend their gratitude to Mario Ordaz who made the recordings available, and to Juan Mayoral for providing research material regarding the stratigraphy of the Mexico City basin. The authors also thank Yoshiaki Hisada for providing the code used to verify SPEED results. Computational resources were made available within the ISCRAB Project "INDQUAKE" funded by CINECA.

Data Availability

The data underlying this article will be shared on reasonable request to the corresponding author.

References

[1] J. G. Anderson. Quantitative measure of the goodness-of-fit of synthetic seismograms. *Proceedings of the 13th World Conference on Earthquake Engineering*, (243):243, 2004.

[2] P. F. Antonietti, I. Mazzieri, A. Quarteroni, and F. Rapetti. Non-conforming high order approximations of the elastodynamics equation. *Computer Methods in Applied Mechanics and Engineering*, 209-212:212–238, 2012.

[3] J. L. Arce, P. W. Layer, J. L. Macías, E. Morales-Casique, A. García-Palomo, F. J. Jiménez-Domínguez, J. Benowitz, and A. Vásquez-Serrano. Geology and stratigraphy of the Mexico Basin (Mexico City), central Trans-Mexican Volcanic Belt. *Journal of Maps*, 15(2):320–332, 2019.

[4] G. Auvinet, E. Méndez, and M. Juárez. *The subsoil of Mexico City vol. III.* Instituto de Ingeniería, UNAM, Ciudad de México, 2017.

[5] P. Y. Bard, M. Campillo, F. J. Chavez-Garcia, and F. Sanchez-Sesma. Mexico earthquake of September 19, 1985 - A theoretical investigation of large- and small-scale amplification effects in the Mexico City valley. *Earthquake Spectra*, 4(3):609–633, 1988.

[6] J. S. Barker, M. Campillo, F. J. Sanchez-Sesma, D. Jongmans, and S. K. Singh. Analysis of wave propagation in the Valley of Mexico from a dense array of seismometers. *Bull. Seismol. Soc. Am.*, 86(6):1667–1680, 1996.

[7] M. Campillo, F. J. Sánchez-Sesma, and K. Aki. Influence of small lateral variations of a soft surficial layer on seismic ground motion. *Soil Dynamics and Earthquake Engineering*, 9(6):284–287, 1990.

[8] F. J. Chávez-García and P. Y. Bard. Site effects in Mexico City eight years after the September 1985 Michoacan earthquakes. *Soil Dynamics and Earthquake Engineering*, 13(4):229–247, 1994.

[9] V. M. Cruz-Atienza, A. Iglesias, J. F. Pacheco, N. M. Shapiro, and S. K. Singh. Crustal structure below the valley of Mexico estimated from receiver functions. *Bull. Seismol. Soc. Am.*, 100(6):3304–3311, 2010.

[10] V. M. Cruz-Atienza, J. Tago, J. D. Sanabria-Gómez, E. Chaljub, V. Etienne, J. Virieux, and L. Quintanar. Long Duration of Ground Motion in the Paradigmatic Valley of Mexico. *Scientific Reports*, 6(December), 2016.

[11] J. A. Diaz-Rodriguez. Effects of repeated loading on the strength of Mexico City clay. In *IVth International Conference on Soil Dynamics and Earthquake Engineering*, Mexico City, 1989.

[12] H. Emmerich and M. Korn. Incorporation of Attenuation Into Time-Domain Computations of Seismic Wave Fields. *Geophysics*, 52(9):1252–1264, 1987.

[13] L. Esteva. Mexico earthquake of September 19, 1985 - Consequences, Lessons, and Impact on Research and Practice, 1988.

[14] L. Evangelista, S. del Gaudio, C. Smerzini, A. D'Onofrio, G. Festa, I. Iervolino, L. Landolfi, R. Paolucci, A. Santo, and F. Silvestri. Physics-based seismic input for engineering applications: a case study in the Aterno river valley, Central Italy. *Bulletin of Earthquake Engineering*, 15(7):2645–2671, 2017.

[15] E. Faccioli, F. Maggio, R. Paolucci, and A. Quarteroni. 2D and 3D elastic wave propagation by a pseudo-spectral domain decomposition method. *Journal of Seismology*, 1:239–248, 1997.

[16] E. Faccioli, A. Tagliani, and R. Paolucci. Effect of Wave Propagation in Random Earth Media on the Seismic Radiation Spectrum. In A. Cakmak and I. Herrera, editors, *Fourth International Conference on Soil Dynamics and Earthquake Engineerin*, Mexico City, 1989. Computational Mechanics.

[17] GCDMX. *Reglamento de construcciones para la Ciudad de México*. Gobierno de la Ciudad de México, 15 de Diciembre de 2017, 2017.

[18] R. Guidotti, M. Stupazzini, C. Smerzini, R. Paolucci, and P. Ramieri. Numerical Study on the Role of Basin Geometry and Kinematic Seismic Source in 3D Ground Motion Simulation of the 22 February 2011 Mw 6.2 Christchurch Earthquake. *Seismological Research Letters*, 82(6):767–782, 2011.

[19] Y. Hisada and J. Bielak. Theoretical method for computing nearfault ground motions in layered half-spaces considering static offset due to surface faulting, with a physical interpretation of fling step and rupture directivity. *Bull. Seismol. Soc. Am.*, 93(3), 2003.

[20] M. Iida and H. Kawase. A comprehensive interpretation of strong motions in the Mexican Volcanic Belt. *Bull. Seismol. Soc. Am.*, 94(2):598–618, 2004.

[21] M. Infantino, I. Mazzieri, A. G. Özcebe, R. Paolucci, and M. Stupazzini. 3D Physics-Based Numerical Simulations of Ground Motion in Istanbul from Earthquakes along the Marmara Segment of the North Anatolian Fault. *Bulletin of the Seismological Society of America*, 110(5):2559–2576, 2020.

[22] A. Jaime. *Características Dinámicas de la Arcilla del Valle México*. Phd thesis, UNAM, 1987.

[23] D. Jongmans, D. Demanet, C. Horrent, M. Campillo, and F. J. Sanchez-Sesma. Dynamic soil parameters determination by geophysical prospecting in Mexico City: Implication for site effect modeling. *Soil Dynamics and Earthquake Engineering*, 15(8):549–559, 1996.

[24] M. Juárez-Camarena, G. Auvinet-Guichard, and E. Méndez-Sánchez. Geotechnical Zoning of Mexico Valley Subsoil. *Ingeniería, Investigación y Tecnología*, 17(3):297–308, 2016.

[25] H. Kawase and K. Aki. A study of the response of a soft basin for incident S, P, and Rayleigh waves with special reference to the long duration observed in Mexico City. *Bull. Seismol. Soc. Am.*, 79(5):1361–1382, 1989.

[26] R. Kosloff and D. Kosloff. Absorbing boundaries for wave propagation problems. *Journal of Computational Physics*, 63(2):363–376, 1986.

[27] R. Marsal and R. Graue. *El subsuelo del lago de Texcoco.* Secretaría de Hacienda y Crédito Público, México, 1969.

[28] J. M. Mayoral, E. Castañon, L. Alcantara, and S. Tepalcapa. Seismic response characterization of high plasticity clays. *Soil Dynamics and Earthquake Engineering*, 84:174–189, 2016.

[29] I. Mazzieri, M. Stupazzini, R. Guidotti, and C. Smerzini. SPEED: SPectral Elements in Elastodynamics with Discontinuous Galerkin: a non-conforming approach for 3D multiscale problems. *International Journal for Numerical Methods in Engineering*, 95:991–1010, 2013.

[30] D. McCallen, A. Petersson, A. Rodgers, A. Pitarka, M. Miah, F. Petrone, B. Sjogreen, N. Abrahamson, and H. Tang. EQSIM—A multidisciplinary framework for fault-to-structure earthquake simulations on exascale computers part I: Computational models and workflow. *Earthquake Spectra*, 37(2):707–735, 2021.

[31] M. Ordaz and S. K. Singh. Source spectra and spectral attenuation of seismic waves from Mexican earthquakes, and evidence of amplification in the hill zone of Mexico City. *Bull. Seismol. Soc. Am.*, 82:24–43, 1992.

[32] E. Ovando-Shelley. Some geotechnical properties to characterize Mexico City Clay. *Pan-Am CGS Geotechnical Conference*, 2011.

[33] E. Ovando-Shelley, A. Ossa, and M. P. Romo. The sinking of Mexico City: Its effects on soil properties and seismic response. *Soil Dynamics and Earthquake Engineering*, 27(4):333–343, 2007.

[34] R. Paolucci, I. Mazzieri, G. Piunno, C. Smerzini, M. Vanini, and A. G. Özcebe. Earthquake ground motion modeling of induced seismicity in the Groningen gas field. *Earthquake Engineering and Structural Dynamics*, 50(1):135–154, 2021.

[35] R. Paolucci, I. Mazzieri, and C. Smerzini. Anatomy of strong ground motion: Near-source records and three-dimensional physics-based numerical simulations of the Mw 6.0 2012 may 29 po plain earthquake, Italy. *Geophysical Journal International*, 203(3):2001–2020, 2015.

[36] M. Romo and E. Ovando-Shelley. Modelling the dynamic behaviour of Mexican clays. In *XI International Conference on Earthquake Engineering*, 1996.

[37] M. P. Romo, A. Jaime, and D. Reséndiz. General Soil Conditions and Clay Properties in the Valley of Mexico. *Earthquake Spectra*, 4(4):731–752, 1988.

[38] F. Sanchez-Sesma, S. Chavez-Pérez, M. Suarez, M. Bravo, and L. Pérez-Rocha. On the seismic response of the valley of Mexico. *Earthquake Spectra*, 4(569-589), 1988.

[39] E. Santoyo-Villa, E. Ovando-Shelley, F. Mooser, and E. Leon-Plata. *Síntesis Geotécnica de la Cuenca del Valle de Mexico*, volume 1. TGC Ingeniería, México, 2005.

[40] H. B. Seed, M. P. Romo, J. I. Sun, A. Jaime, and J. Lysmer. Mexico earthquake of September 19, 1985 - Relationships between soil conditions and earthquake ground motions, 1988.

[41] T. H. Seligman, J. Alvarez-Tostado, J. L. Mateos, and J. Flores. Resonant response models for the Valley of Mexico-I; the elasic inclusion approach. *Geophysical Journal International*, pages 789–799, 1989.

[42] N. M. Shapiro, M. Campillo, A. Paul, S. K. Singh, D. Jongmans, and F. J. Sánchez-Sesma. Surface-wave propagation across the Mexican Volcanic Belt and the origin of the long-period seismic-wave amplification in the Valley of Mexico. *Geophysical Journal International*, 128(1):151–166, 1997.

[43] N. M. Shapiro, K. B. Olsen, and S. K. Singh. On the duration of seismic motion incident onto the Valley of Mexico for subduction zone earthquakes. *Geophysical Journal International*, 151(2):501–510, 2002.

[44] N. M. Shapiro, S. K. Singh, D. Almora, and M. Ayala. Evidence of the dominance of higher-mode surface waves in the lake-bed zone of the Valley of Mexico. *Geophysical Journal International*, 147(3):517–527, 2001.

[45] S. K. Singh, J. Lermo, T. Dominguez, M. Ordaz, J. M. Espinosa, E. Mena, and R. Quaas. A study of amplification of seismic waves in the valley of Mexico with respect to a hill zone site, 1988.

[46] S. K. Singh, E. Mena, and R. Castro. Some aspects of source characteristics of the 19 September 1985 Michoacan earthquake and ground motion amplification in and near Mexico City from strong motion data. *Bull. Seismol. Soc. Am.*, 78(2):451–477, 1988.

[47] S. K. Singh, A. Mori, E. Mena, F. Krüger, and R. Kind. Evidence for anomalous body-wave radiation between 0.3 and 0.7 Hz from the 1985 September 19 Michoacan, Mexico earthquake. *Geophysical Journal International*, 101(1):37–48, 1990.

[48] S. K. Singh and M. Ordaz. On the Origin of long coda observed in the lake-bed strong-motion records of Mexico City. *Bull. Seismol. Soc. Am.*, 83(3):1298–1306, 1993.

[49] S. K. Singh, R. Quaas, M. Ordaz, F. Mooser, D. Almora, M. Torres, and R. Vásquez. Is there truly a “hard” rock site in the Valley of Mexico? *Geophysical Research Letters*, 22(4):481–484, 1995.

[50] S. K. Singh, L. Quintanar-Robles, D. Arroyo, V. M. Cruz-Atienza, V. H. Espíndola, D. I. Bello-Segura, and M. Ordaz. Lessons from a small local earthquake (Mw3.2) that produced the highest acceleration ever recorded in Mexico City. *Seismological Research Letters*, 91(6):3391–3406, 2020.

[51] C. Smerzini and K. Pitilakis. Seismic risk assessment at urban scale from 3D physics-based numerical modeling: the case of Thessaloniki. *Bulletin of Earthquake Engineering*, 16(7):2609–2631, 2018.

[52] C. Smerzini and M. Villani. Broadband numerical simulations in complex near-field geological configurations: The case of the 2009 Mw 6.3 L'Aquila earthquake. *Bull. Seismol. Soc. Am.*, 102(6):2436–2451, 2012.

[53] SSN. Secuencia sísmica del 12 al 18 de Julio De 2019, Cuenca De México (M 3.0). Technical report, Servicio Sismológico Nacional, Instituto de Geofísica, Universidad Nacional Autónoma de México, Ciudad de México, 2019.

[54] SSN. *Catálogo de sismos.* UNAM, I. d. G., Servicio Sismológico Nacional. http://www2.ssn.unam.mx:8080/catalogo/%0A%0A, 2020.

[55] M. Stupazzini, M. Infantino, A. Allmann, and R. Paolucci. Physics-based probabilistic seismic hazard and loss assessment in large urban areas: A simplified application to Istanbul. *Earthquake Engineering & Structural Dynamics*, 50(1):99–115, 2021.

[56] M. Stupazzini, R. Paolucci, and H. Igel. Near-fault earthquake ground-motion simulation in the Grenoble Valley by a high-performance spectral element code. *Bull. Seismol. Soc. Am.*, 99(1):286–301, 2009.

MOX Technical Reports, last issues

Dipartimento di Matematica
Politecnico di Milano, Via Bonardi 9 - 20133 Milano (Italy)

87/2021 Both, J.W.; Barnafi, N.A.; Radu, F.A.; Zunino, P.; Quarteroni, A.
Iterative splitting schemes for a soft material poromechanics model

86/2021 Possenti, L.; Cicchetti, A.; Rosati, R.; Cerroni, D.; Costantino, M.L.; Rancati, T.; Zunino, P.
A Mesoscale Computational Model for Microvascular Oxygen Transfer

85/2021 Cavinato, L., Gozzi, N., Sollini, M., Carlo-Stella, C., Chiti, A., & Ieva, F.
Recurrence-specific supervised graph clustering for subtyping Hodgkin Lymphoma radiomic phenotypes

89/2021 Boulakia, M.; Grandmont, C.; Lespagnol, F.; Zunino, P.
Reduced models for the Poisson problem in perforated domains

88/2021 Kuchta, M.; Laurino, F.; Mardal, K.A.; Zunino, P.
Analysis and approximation of mixed-dimensional PDEs on 3D-1D domains coupled with Lagrange multipliers

84/2021 Torti, A.; Galvani, M.; Urbano, V.; Arena, M.; Azzone, G.; Secchi, P.; Vantini, S.
Analysing transportation system reliability: the case study of the metro system of Milan

83/2021 Colasuonno, F.; Ferrari F.; Gervasio, P.; Quarteroni, A.
Some evaluations of the fractional p-Laplace operator on radial functions

80/2021 Sollini, M., Bartoli, F., Cavinato, L., Ieva, F., Ragni, A., Marciano, A., Zanca, R., Galli, L., Pai
[18F]FMCH PET/CT biomarkers and similarity analysis to refine the definition of oligometastatic prostate cancer

79/2021 Ferraccioli, F.; Sangalli, L.M.; Finos, L.
Some first inferential tools for spatial regression with differential regularization

82/2021 Massi, M.C.; Ieva, F.
Learning Signal Representations for EEG Cross-Subject Channel Selection and Trial Classification